Tellus (1995), 47A, 998–1012
Printed in Belgium – all rights reserved

TELLUS
ISSN 0280–6495

On the frequency-wavenumber structure of the tropical ocean/atmosphere system

By T. P. BARNETT[1]*, M. LATIF[2], N. GRAHAM[1] and M. FLÜGEL[2], [1]*Climate Research Division, Scripps Institution of Oceanography, La Jolla, CA 92093-0224, USA*; [2]*Max Planck Institut fur Meteorologie, Hamburg, Germany*

(Manuscript received 10 November 1994; in final form 10 April 1995)

ABSTRACT

Simulations with an ocean general circulation model and a hybrid coupled model reproduce well the observed principal spatial mode (PSM) of variation of the tropical Pacific ocean/atmosphere system. The model results show the origins of the PSM to be a coupled ocean/atmosphere mode and suggest this phenomenon is not a natural mode of the tropical Pacific Basin alone. Air-sea interactions amplify the mode variability by a factor of 5–6 over the strength it would have in a purely random atmosphere and so it obtains climatological importance. These same interactions introduce the PSM to the atmosphere. The PSM of interannual variability is not directly driven by the annual cycle. But its time scale does depend importantly on the fact that the ocean-atmosphere coupling strength varies with respect to the annual cycle. The mode appears to be rather sharply peaked in wave number space but broadbanded in frequency space so that identifying it with a temporal designator, as has been done in the past is apt to be misleading.

1. Introduction

Large-scale air-sea interactions play a major role for the generation of climate variability in the tropical Pacific (Bjerknes, 1969). As described by several authors, these interactions take place on a variety of time scales (Barnett, 1991) which we will refer to as modes of variability. Of these modes, the most prominent is the annual cycle in the eastern equatorial Pacific. The existence of this mode is partly due to coupled processes (Horel, 1982; Philander, 1990; Neelin, 1991). There also exists interannual variability (Rasmusson and Carpenter, 1982) which shows variability on a quasi-biennal (QB) time scale (Rasmusson et al., 1990) and at lower frequencies (Barnett, 1991). Theoretical work shows that unstable air-sea interactions on the time scales noted above are possible for a large expanse of model parameter space (Battisti, 1988; Battisti and Hirst, 1989; Schopf and Suarez, 1988; Philander et al., 1992; Neelin, 1991; Neelin and Jin, 1993; Neelin et al., 1992), with quite different spatial and temporal characteristics for different locations of the model coefficients in parameter space. Thus, although much progress has been made in deriving a theory of air-sea interactions in the tropical climate system, the observational evidence for the validity of certain approximations in the above body of work remains a controversial issue.

Earlier work by Latif et al., 1992 (hereafter L92) investigated and described three fundamental temporal frequencies of variability or modes in the ocean-atmosphere system of the tropical Pacific Ocean. These frequencies were defined objectively by a simultaneous Principal Oscillator Pattern (POPs) analysis (Hasselmann, 1988; von Storch et al., 1988; and Xu and von Storch, 1990, Appendix A) of the observed fields of wind stress, sea surface temperature (SST) and ocean heat content. The periods resulting from this analysis were roughly 12, 22 and 34 months, the annual cycle (AC), quasibiennial (QB) and low frequency (LF) modes, respectively. The first time scale was simply the annual cycle. Of the latter two time

* Corresponding author.

scales, the one near 34 months is the one of interest in this study. It has been shown to be a fundamental constituent of the El Niño-Southern Oscillation (ENSO) phenomenon (see below). The goal of the present paper is to determine the physical origins of this important mode of variation in the tropical climate system and its frequency-wavenumber structure.

Past work describing the above modes has generated some confusion since the temporal designators (QB and LF) do not have precise periods associated with them. So different investigators often seem to apply different temporal designators to the same mode, hence the confusion. The fundamental problem is that the modes are not periodic and are (generally) associated with a red spectrum; or if spatial peaks can be found, they are highly dependent on record length, location, etc. In the present paper we key on the spatial patterns of variability as the fundamental description of the modes. Specifically, we will investigate the most energetic mode which we term the principal spatial mode or PSM. As will be shown, it can have temporal periods ranging from 26–40 months and so could be given a temporal designator for the QB or LF modes noted above.

2. The PSM mode in observations

The work of L92, as it pertains to the PSM, is summarized briefly here for it is vital to evaluating the reality of model results to be presented later.

2.1. Data and procedures

It is well-known from linear stability analysis that the most important quantities in tropical air-sea interactions are zonal surface wind, sea surface temperature (SST), and upper ocean heat content (Hirst, 1986; Neelin, 1991). With this in mind, these important quantities were subjected to a POPs analysis (see Appendix A). The analysis period extends from 1967 to 1986. The SST data were described by Graham and White (1990) and are based on the COADS data set. The zonal surface wind stress was taken from the Florida State University (FSU) data set (Goldenberg and O'Brien, 1981; Legler and O'Brien, 1984). As a measure of upper ocean heat content (sea level surrogate) we use the depth of the 20°C-isotherm. This data set is comprised of a re-analysis of the temperature/depth data based upon more than 150,000 vertical profiles of temperature archived at the Japan Far Seas Fisheries Research Laboratory (JFSFRL) and at the Scripps Institution of Oceanography (SIO). SST and zonal wind stress cover the domain 124° E to 80° W. The subsurface data were available only for the region 120° E to 140° W. The meridional domain extends from 24° N to 24° S. The data coverage for the 20°C isotherm data set, especially during the first half of the analyzed period, is poor, resulting in large spatial and temporal gaps. We filled these gaps in our analysis by assuming zero anomaly after removing the annual mean value. Since the heat content data were available on a bimonthly basis only, the entire analysis was based on bimonthly data. For this purpose, the monthly SST and zonal

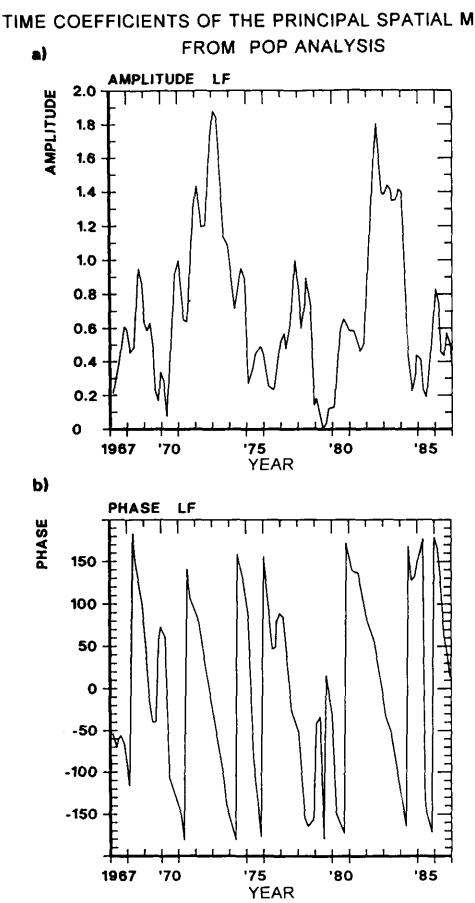

Fig. 1. Amplitude (a) and phase (b) time series of the Principal Spatial Model POP.

stress data were transformed into bimonthly values.

2.2. *Results*

The most energetic interannual POP mode, the PSM, accounting for about 24% of the variance in the data, has a rotation time of between 26–39 months (Section 6) and a decay time of about 4 years. This POP mode was already described partly by Latif et al. (1993). The POP coefficient time series of the PSM indicates a clear relationship to the ENSO cycle. The zero-lag correlation of the real part POP coefficient time series with the NINO3 SST index is 0.76, while the lag-8 (months) correlation of the imaginary part is 0.61, with the POP coefficient time series leading the NINO3 index. Thus, the PSM accounts for most of the ENSO-related variability. This is also supported by the study of Latif et al. (1993), who show that the mode can be successfully exploited for ENSO predictions up to lead times of about one year. The amplitude time series of the PSM POP (Fig. 1, upper) exhibits the most energetic times during the periods 1972/1973 and 1982/1983. The corresponding phase-time series clearly shows the process is not simple periodic (Fig. 1, lower).

The spatial patterns of the PSM POP emphasize also its close connection to the ENSO phenomenon (Fig. 2). The real part patterns (righthand panels) show the familiar anomaly characteristics observed during the height of the extremes of ENSO, with maximum SST anomalies in the eastern equatorial Pacific, westerly wind stress anomalies, centered at the equator near the dateline, and the characteristic drop of heat content in the entire western equatorial Pacific. The imaginary part patterns (left-hand panels) show conditions about 9 months earlier. The dominant feature in these "precursor" patterns is a signal in upper ocean heat content at the equator, centered near 160° W. This signal propagates eastward with a speed of about 25 cm/s, which is about one order of magnitude slower than the gravest baroclinic Kelvin wave speed.

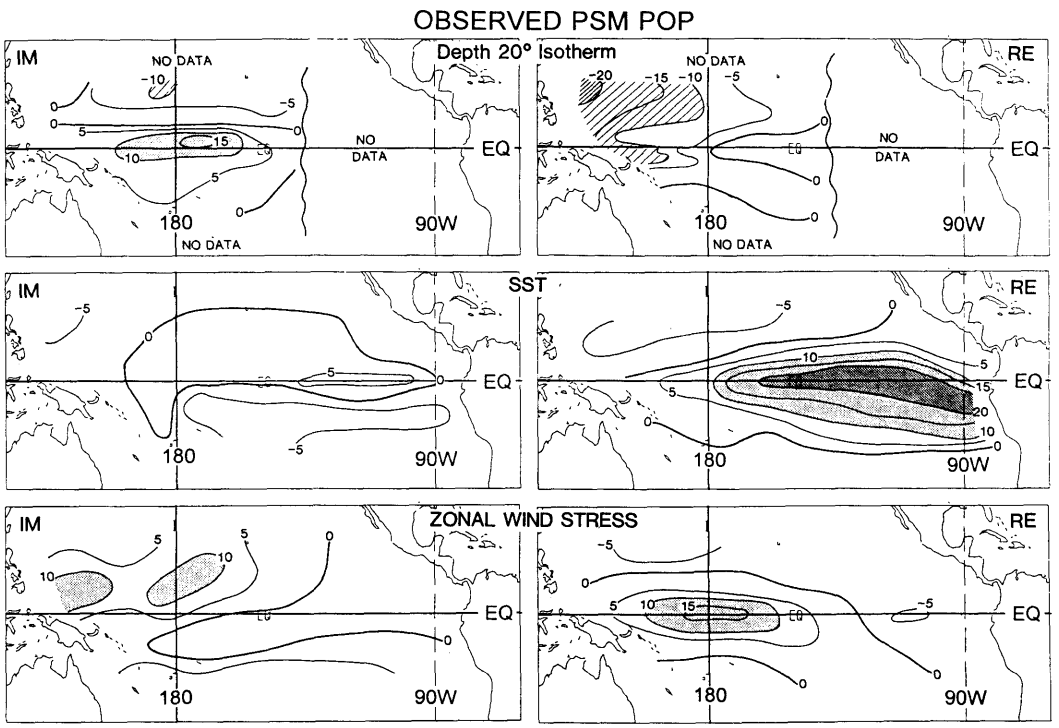

Fig. 2. Spatial patterns of the PSM POP. Left: imaginary part patterns. Right: real part patterns. Upper: depth of 20°C isotherm, a surrogate for sea level. Middle: sea surface temperature. Lower: zonal wind stress.

The evolution of anomalies in the PSM is broadly consistent with equatorial wave dynamics as summarized by the conceptual model of "delayed action oscillation" (Schopf and Suarez, 1988; Graham and White, 1988; Cane et al., 1990; Chao and Philander, 1993) and a coupled ocean/atmosphere mode (Neelin, 1991; Neelin and Jin, 1993). According to this picture, the ocean is not in equilibrium with the atmosphere and has a memory to past winds, as described by Cane and Sarachik (1981). Phase differences between upper ocean heat content on the one hand and SST and wind on the other hand are crucial to maintain the oscillation. Examples of these features are readily apparent in observations displayed in the Climate Analysis Center's *Climate Diagnostics Bulletin*, e.g., see the panels on equatorial section heat content, SST anomaly, and 850 mb wind anomaly longitude-time diagrams for the last several El Niño events.

3. The PSM in an ocean model

Prior to using a series of ocean general circulation model (OGCM) experiments to dissect the PSM, we first wish to demonstrate that the OGCM can reproduce the observed features described above. The OGCM to be used in this study is the nonlinear primitive equation version of the Hamburg tropical Pacific Ocean model (Latif, 1987) that calculates the three-dimensional current field, sea level and SST. The model has realistic horizontal geometry with a zonal grid spacing of 670 km and a meridional resolution of 50 km near the equator, expanding to about 400 km at the northern/southern boundaries (30°N/30°S). There are thirteen irregularly spaced levels in the vertical, with 10 of the levels in the upper 300 m. Vertical mixing is accomplished through use of a Richardson's number dependent formalism (Pacanowski and Philander, 1981). In the experi-

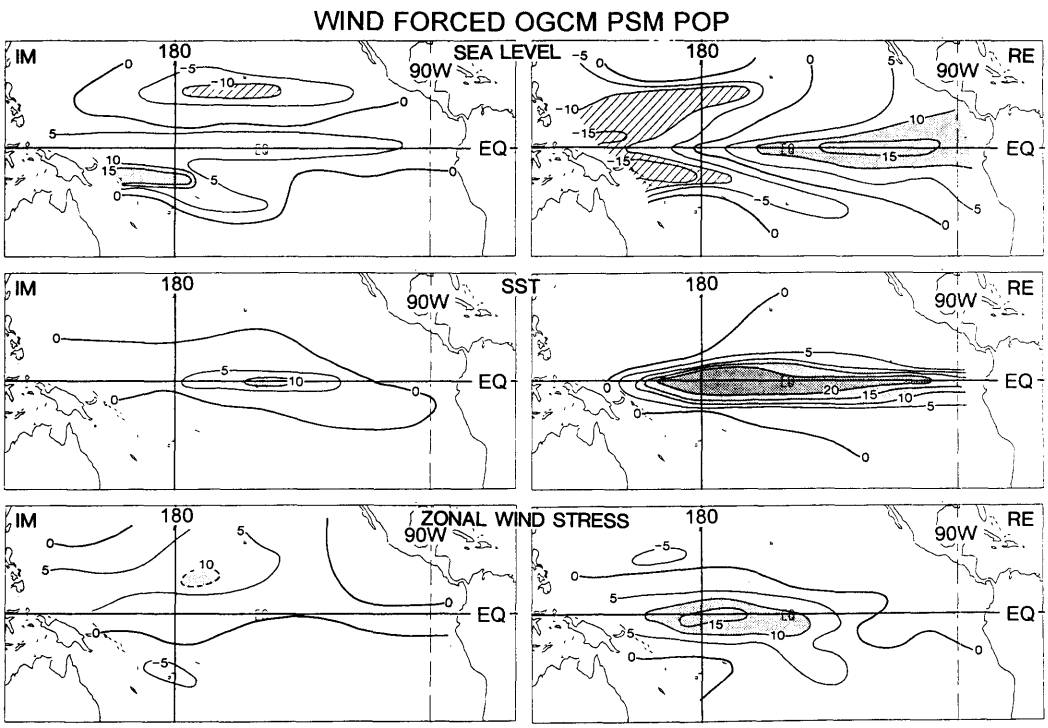

Fig. 3. Principal oscillator pattern (POP) for the PSM obtained from the OGCM forced by 29 years of observed wind stress. This POP was derived from the multivariate field of sea level (upper), SST (middle), and zonal wind stress (lower). See Fig. 2 legend.

ments to be described below, the model was forced with the observed, monthly FSU windstress for the period 1962–1990 (*cf.* Goldenberg and O'Brien, 1981). This simulation reproduced fairly well the observed broad-band SST variations over the period of interest (Miller et al., 1993).

The SST, sea level and wind stress fields resulting from the above model run were analyzed in exactly the same manner as were their observational counterparts in L92. There were only two meaningful interannual POPs modes that resulted from this analysis, and they had periods of 24 and 35 months, respectively. The spatial POP pattern associated with the most energetic POP mode from the OGCM run is shown in Fig. 3. It bears a reasonable resemblance to the PSM POP pattern found from the observations; compare with Fig. 2. The degree of similarity was quantified by computing the complex pattern correlation between the (complex) LF POP from the data and the forced model run, i.e., between Fig. 2 and Fig. 3. The modulus of this correlation, which is a measure of the similarity between the POPs, was 0.77. The temporal correlation of the associated (complex) POPs coefficients was 0.65, a value we would have expected from the earlier model evaluation of Miller et al., 1993. Both values are significant at 0.05 or more from those expected from a set of random numbers. There are also clear differences between the two analyses, particularly in the eastern and western margins of the ocean. Some of this is likely due to model resolution, both horizontal and vertical. But it is also true that the heat content is only poorly observed and that may be part of the problem on the upper panels. All in all, given the strong correlations noted above, we conclude that the model forced by the observed winds has done a reasonable job of reproducing the temporal evolution and spatial structure of the PSM found in the observations.

4. PSM mode without air/sea coupling

In this section we investigate two ideas. The first is the degree to which the PSM signal under discussion depends on air/sea coupling for its existence as suggested by many earlier studies. Second, we wish to see if such a mode results from an interaction of the annual cycle with itself. The answers to both questions were obtained from three simulations with the OGCM.

In the first simulation, 1000 years in length, the OGCM was forced by a combination of the annual cycle and noise, $N(\boldsymbol{x}, t)$, that was "white" in time and "white" in space, with a spatially uniform standard deviation of 0.25 dynes/cm^2, a typical value for the FSU stress data set. Thus, N is completely uncorrelated in both $\boldsymbol{x}$ and t. We refer to this run as the "annual cycle/white-white" run or ACWW. In the second simulation, the model was forced with the annual cycle of wind stress plus a noise field given by:

$$N(\boldsymbol{x}, t) = \sum_{i=1}^{10} a_i(t)\, e_i(\boldsymbol{x}),$$

where $e_i(\boldsymbol{x})$ is the ith empirical orthogonal function of the FSU anomalous wind stress data set (1965–1988) and $a_i(t)$ is a random principal component constructed such that

$$a_i(t_n) = r_n(0, \lambda_i),$$

where r_n is the nth random number drawn from a population with zero mean and variance λ_i, i.e., variance proportional to the ith eigenvalue from the wind stress EOF analysis. Thus the forcing field of the anomalous wind stress was constructed to be "red in space and white in time". We will refer to this experiment as the "annual cycle/red-white" or ACRW forced run. The third experiment is identical to the second, but now the seasonal cycle of wind forcing was replaced at each gridpoint by the annual average stress appropriate to that grid point. We refer to this experiment as the "annual average/red-white" or AARW run. The same set of random numbers was used in each of the latter two runs to clearly delimit the role of the annual cycle in the experiments.

The numerical experiments are summarized succinctly below and in Fig. 4 which shows the power spectrum of the SST anomaly for region NINO3 for the last two runs. We draw three major conclusions:

(i) The "white-white" run (ACWW) produced a power spectrum (not shown) of SST and sea level in NINO3 that was "red" except for strong annual and semi-annual peaks. Apparently, the ocean cannot generate by itself the PSM, i.e., it is not a

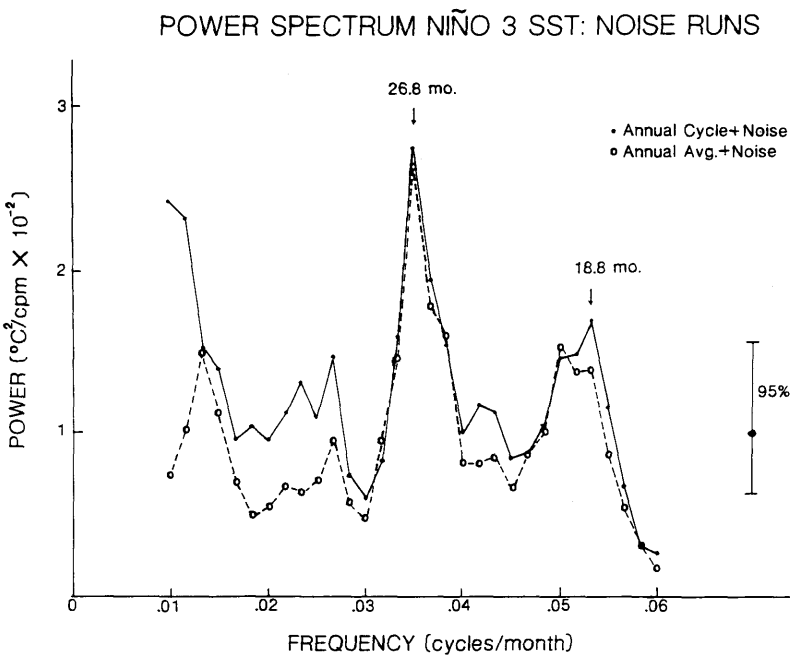

Fig. 4. Power spectra of NINO3 SST anomaly from 50-year OGCM runs forced by spatially red and temporally white anomalous wind stress. One run also included the regular seasonal cycle of wind stress (solid dot), while the other used annual average stress as climatological forcing (open circle). The NINO3 region is between 90–150° W and 5° N–5° S.

linear eigenmode of the ocean. This result from a numerical simulation is in agreement with the many theoretical studies mentioned above.

(ii) The power spectra for ACRW and AARW show a major peak at 26.8 months period and a secondary peak near 19 months (Fig. 4). The lower frequency peak is significant (0.05 level), but the higher frequency peak is only marginally meaningful. The POP analysis of these noise forced OGCM runs produced an unstable periodicity, using the standard POP estimate, that varied between 24 and 29 months depending on the length of record used. The spatial patterns for the POP (Fig. 5) were identical to each other and were quite similar to those obtained for the PSM derived from the wind forced run from the OGCM (Section 3.0); the associated pattern correlation was 0.82. In addition, the POP pattern correlation between the spatially red noise forced OGCM runs, the latter two simulations, and the comparable observed POP from Section 2 (Fig. 2) was 0.77. In essence then, the principal mode of the ACRW and AARW noise forced runs was the PSM described above and in Section 2. The 10–15% difference in time scale estimates, is likely within the uncertainty of the individual estimates although we cannot show this rigorously (cf. Section 6).

The results clearly suggest that the addition of large scale spatial coherence to the temporally stochastic wind forcing produces patterns of ocean variability much like those observed. By specifying the large scale spatial structure of the wind patterns, which was presumably induced in the FSU data by the ENSO signal itself, one might say we have provided the desired answer to the OGCM. Put another way, the impression of spatially fixed patterns of wind stress, effectively filters the ocean dynamics in a way that allows only the observed PSM (ENSO) signal, even though the temporal variability is purely random. The wave number or k-dependence of this signal combined with the mean properties of the model ocean automatically select the appropriate time scale; essentially forcing waves on only a localized portion of a dispersion relation.

We note in passing that in the real world, the wavenumber spectrum of the wind stress is not white, e.g., the west wind bursts associated with the

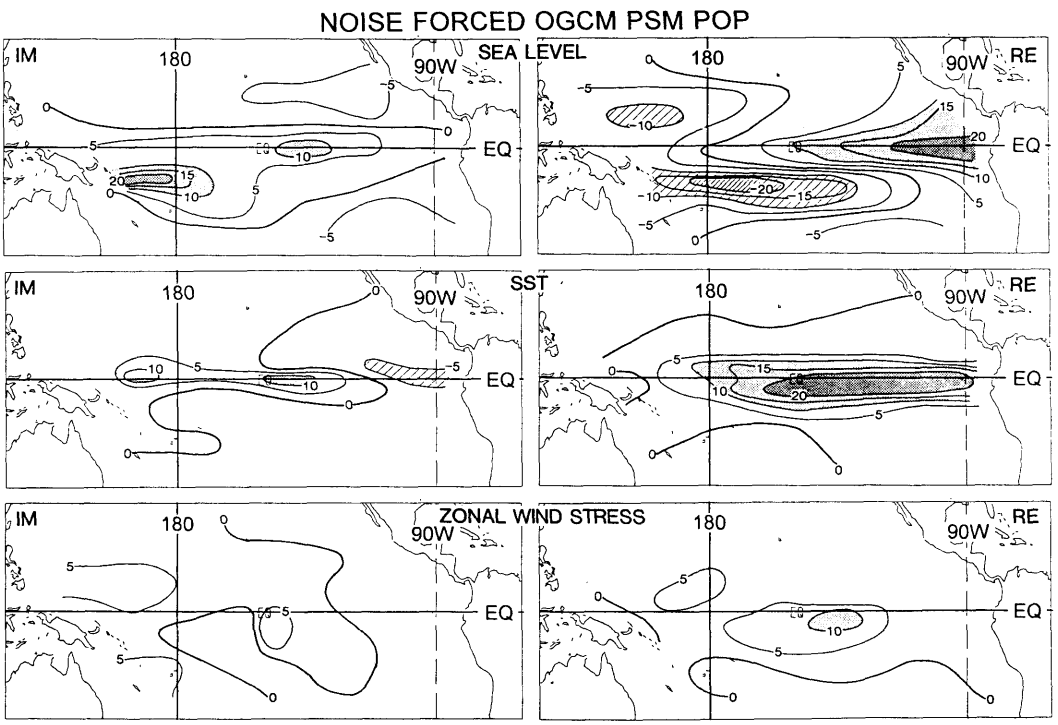

Fig. 5. As Fig. 2, but from the OGCM forced by wind stress that is "red" in space and "white" in time.

Madden-Julian oscillation. To represent this latter situation, we high pass filtered the observed wind stress field to retain time scales less than 12 months and repeated the ACRW experiment described above. The PSM was obtained as the most energetic mode of variability.

(iii) The power spectra are nearly identical over the frequency range of interest, so the inclusion of the annual cycle (ACRW), or the lack thereof (AARW), had little to do with variability outside its immediate frequency band. Thus, the idea that the PSM variations are somehow forced *directly* by the annual cycle, e.g., are a simple subharmonic of the annual cycle, is not supported by the numerical simulation. We repeated the ACRW experiment for another realization of the white noise forcing and obtained essentially the same result as shown on Fig. 4.

The very low-frequency behavior of the model seen in the spectra is spurious. It arises from a slow drift associated with the lack of a long term balance in the heat budget of the model. This is induced largely by the model's failure to properly compensate for heat which should (in nature) be transported meridionally by the ocean but cannot be due to the solid "walls" at 30° N/S. Apparently the combination of diffusion and pseudo-heat flux parameterizations are not quite energy conserving over the model domain. This problem should have no impact on the use of the OGCM for ENSO-related studies.

In summary, the PSM is not a fundamental mode of oscillation of the equatorial Pacific in and of itself. Rather, it is the large-scale anomalous structure of the wind forcing that couples with the ocean (see below) to produce the oscillation. The simulations suggest that the annual cycle, by itself, has little or no role in directly forcing the LF variations we have found in the OGCM.

5. The role of ocean-atmosphere coupling

In this section, we investigate the role of ocean-atmosphere coupling in the PSM. The results from the preceding section would, at first glance, appear

to rule out such a coupling in the noise runs, but this is not the case. The random wind field used in the above experiments is theoretically composed of an infinite number of Fourier components having different frequencies, wave numbers and directions of propagation. Thus, in analogy to the resonant theory of wind wave generation of Phillips (1962), there will be some element of the forcing field that could move and resonantly interact with the ocean features that comprise the PSM. These elements of the wind field would thus appear to be phase locked to the ocean, just as is observed in nature.

The principal tool we will use in the following discussion is the hybrid coupled model (HCM) described by Barnett et al. (1993, hereafter B93). The ocean component of the HCM consists of the OGCM used in the earlier sections of this paper. The atmospheric component is a statistical model that specifies the anomalous wind stress from information on anomalous SST provided by the ocean model. In effect, the atmosphere in the HCM is a "slave" to the ocean without any internal dynamics. The seasonal cycle for ocean variables is computed by the OGCM, while the seasonal cycle of atmospheric forcing is specified; the atmospheric model is thus an anomaly model. A critical element of the atmospheric model is that the ocean-atmosphere coupling coefficients were computed independently from the observed SST and wind stress data for each month of the year. It was shown in B93 that the HCM did a reasonable job of reproducing both the space and temporal variability observed in the ocean and atmosphere of the tropical Pacific. It also produced reasonable forecasts of large ENSO events at lead times out to 18 months in advance. In short, the HCM appears an adequate tool for studying the PSM type of phenomenon.

5.1. HCM and the PSM

The HCM had a somewhat chaotic behavior, but showed a definite preference in extended integrations for oscillation at or near periods of two or three years. As noted in B93, the spatial structure of this behavior was very similar to that observed in both the real SST and sea level fields, independent of whether the HCM was oscillating at 2 or 3 year periods. This is partially illustrated in Fig. 6. It is also important to note that the POPs results referred to in that illustration bear a marked similarity to those obtained from analysis of the 29-year integration of the OGCM forced by the observed winds (Section 3). The pattern correlation between the PSM POP from the wind forced run and the PSM POP from a 50 year segment of HCM run with either the 2- *or* 3-year period, was 0.84. Comparing the HCM POP with that derived from the observations yields a complex pattern correlation with modulus 0.60 (between Figs. 6 and 2). There are differences in the patterns, especially along the equator, that are likely due to poor representation of upwelling (resolution again). But, on balance, we conclude that the spatial response of the HCM is essentially the PSM seen in nature and in the wind forced OGCM. This statement is true whether one is dealing with the HCM fields that have a predominantly 2- *or* 3-year period. As noted in the Introduction, using a temporal descriptor (e.g., LF) to represent this mode of variability is clearly confusing and not ideal. We note it here mainly for historical continuity.

The HCM runs can be compared with the noise forced run (Section 4) to estimate the degree to which air/sea coupling enhances the PSM. In the former runs the coupling is both explicit and strong, while in the noise run it is necessarily weak (no explicit coupling). A lower limit on the signal enhancement was estimated as follows: Power spectra of 50 years time series of SST in NINO3 from the HCM were computed using exactly the same procedures as used in the construction of Fig. 4. Given the time scale ambiguity in the HCM associated with the PSM, separate 50-year segments having predominantly 2-year and 3-year variability were analyzed. The peak energies of the HCM spectra were roughly 30 times those found in the noise run. The physical mechanisms responsible for this amplification were explained in B93. Based on the relative magnitudes of the spectral peak energies (30 to 1), one may surmise that the explicit ocean-atmosphere coupling enhances the amplitude of the PSM variations by roughly a factor of $\sqrt{30}$ or 5–6 over what it would have been in the presence of an atmosphere whose temporal variations were purely random (no explicit feedback).

In summary, the role of discrete, explicit air-sea interactions in the PSM is that of an amplifier and a coupler. Without amplification, the role of the PSM variations in interannual climate change, e.g., ENSO, would likely be unimportant. While

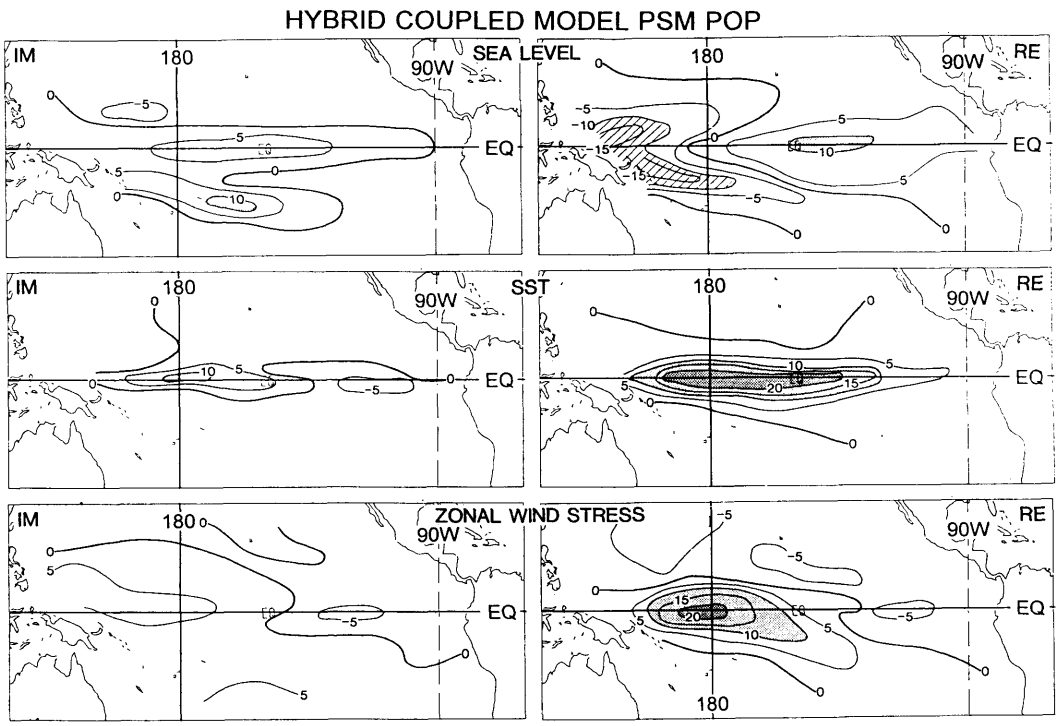

Fig. 6. POP associated with PSM in the hybrid coupled model (HCM). The analysis was performed on a multivariate data set composed of SST, sea level and zonal wind stress from a 50-year run of the HCM. See Barnett et al. (1993) for more details on the model and associated analysis.

performing the role of amplifier, these same interactions provide the close linkage between the ocean and atmosphere that allows the coupled mode to exist and influence large regions of the planet (cf. Barnett, 1991, Figs. 2, 3 and 5).

5.2. *The role of seasonality in atmospheric forcing*

The seasonal cycle does play an important role in the PSM variability but, as we have seen above, it is not what one might term a direct role. The role of seasonality in producing the LF variations has been demonstrated by two additional numerical experiments with the HCM. Both runs start from a comparable, but not identical, initial condition (t_0) obtained from, say, July of a control run. In the first experiment, the integration was allowed to continue beyond t_0, with normal changes in the annual cycle, i.e., the seasonal cycle component of the wind stress was allowed to evolve as appropriate to the time of year. The wind anomalies, however, were computed by the atmospheric model under the assumption of a perpetual July, i.e., there was no seasonality in the atmospheric feedback. In the second experiment, both the seasonal component of the wind and the atmospheric anomaly model were held to July, i.e., a perpetual July was imposed on both the seasonal cycle and the atmospheric feedback.

The temporal character of both experiments are demonstrated clearly by inspecting the time history of SST in region NINO3 (Fig. 7) for the first 26 years of the coupled integrations. The comparable time history for the continuation of the control run, which included full seasonality in both the wind stress annual cycle specification and in the coupling coefficients of the anomalous atmospheric model, is shown for comparison.

A highly regular 5-year oscillation appears in both the upper panels*. Yet the pattern correlation between the lead POP of the perpetual July run

* This is one of the characteristic ENSO time scales estimated by other authors.

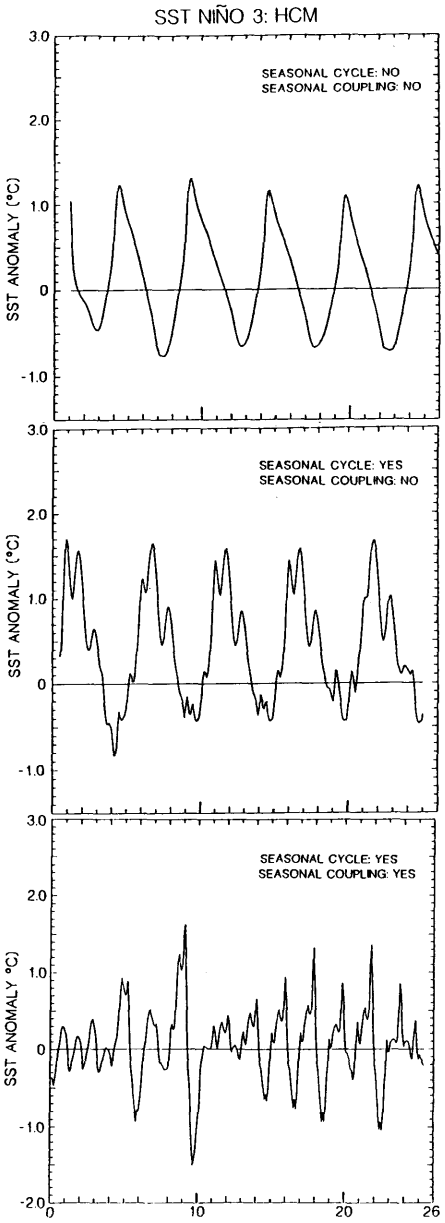

Fig. 7. Time series of NINO3 SST anomaly from HCM runs with various forms of seasonal wind forcing: No seasonal cycle and no seasonal dependence in the anomalous ocean/atmosphere coupling (upper); seasonal cycle forcing from climatology and no seasonal dependence in the anomalous ocean/atmospheric coupling (middle); seasonal cycle forcing from climatology and seasonal dependence in anomalous ocean/atmosphere coupling (lower).

(upper) and the lead POP of the standard coupled control run (lower) was 0.66, so again the spatial response of the PSM is robust to different temporal forcing. Inclusion of the seasonal cycle in the specified background mean state (middle panel) did little to affect this finding aside from adding temporal variability at the annual time scale. Allowing for seasonality in the ocean-atmosphere coupling (lower panel) produced irregular and higher frequency variability. In the HCM, at least, the seasonality in the degree of ocean-atmosphere coupling is critical to determining the time scale of the PSM variability. The annual cycle, by itself, apparently does not directly participate in the PSM.

Brier (1978) and Nicholls (1978, 1984) have suggested that low-frequency variability could be induced by an ocean-atmosphere interaction whose strength (or sign) varied with the annual cycle. In concept, at least, this was also Meehl's (1987, 1992) suggestion. That is exactly the type of mechanism at work in the HCM. As described in B93, the wind forcing from the atmospheric model has a strong seasonal asymmetry (Fig. 8) of the type that should produce variability at a frequency near the first subharmonic of the annual cycle. Forcing near this frequency band will interact in near resonance with the natural mode described in Section 4. Such a mechanism would produce a negligible nonlinear interaction coefficient between the resultant low frequency time scale and the annual cycle as found by Barnett (1991) and in L92.

We note that the behavior of the HCM is sensitive to variation in coefficients and background mean state (like the Lamont model, Zebiak and Cane, 1991; Graham et al., 1994). Thus, its behavior in the non-seasonal mode (Fig. 7, upper) is interesting but represents a very different model from that with seasonally dependent anomalous forcing. The latter model appears closer to reality since it more closely reproduces the observed time scales of variability.

In summary, the results presented here, plus those reported by earlier workers, support the hypothesis that the time scale of the PSM variability is associated with the seasonally varying manner in which the ocean and atmosphere interact with each other. The interested reader is referred to B93 for a more detailed description of the seasonal character in the HCM.

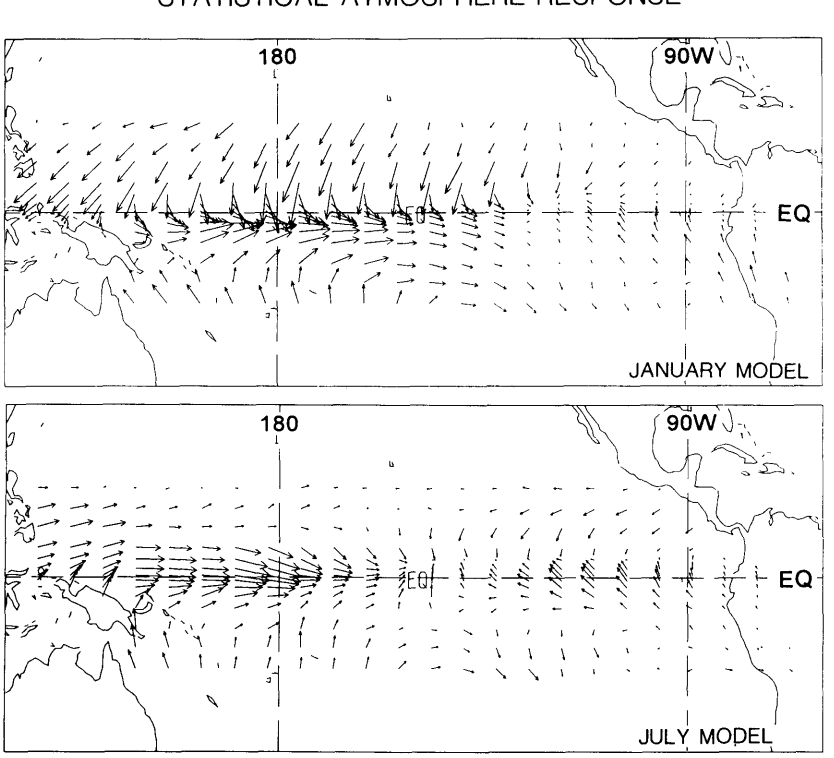

Fig. 8. Anomalous wind stress field produced by an observed warm SST anomaly (February 1992) from the atmospheric component of the HCM: upper, using January coefficients; lower, using July coefficients.

6. The time scale

In general, the estimates of spatial structure of the PSM we obtained from the different numerical experiments and observations are consistent with each other. However, the temporal variability, as denoted by the estimated period of the mode, is more variable than we would have expected a priori. The reason for this may lay in the analysis methods themselves.

In a POPs analysis, there are four different ways to obtain the characteristic time scale (see Appendix B for a description and definition of terminology). They can give rather different answers (cf. Fig. 9). For example, the regular POP period and energy weighted phase estimates both gave periods 39 months while the amplitude weighted cumulative phase method gave 34 months for the observations. All of these measures are subject to overestimation in the presence of a few large amplitude events (e.g., 1982–1983 ENSO). The unweighted cumulative phase estimation procedure, which is unaffected by large magnitude events, gave a period of 27 months. So the POP-estimated time scale for the PSM lies in the range 27 to 39 months; the range depending solely on analysis method. We show also in Fig. 9 similar estimates for the QB mode time scale obtained in L92. Note the similar scatter in estimation of the QB mode. There is, however, a clear temporal separation of the QB and PSM modes.

The spectral estimate (from Fig. 4) from the noise forced OGCM run gave a characteristic PSM time scale of roughly 27 ± 1 months while the POP period of that run gave a 29 month period. Combining these results with those just above suggests we can assign a time scale of 26–39 months to the PSM. Note the lower end of this time span includes what many authors have called the quasi-biennial period (Trenberth, 1975; Quiroz, 1983; Rasmusson et al., 1990; Yasunari, 1989).

The highly unsatisfactory situation with time

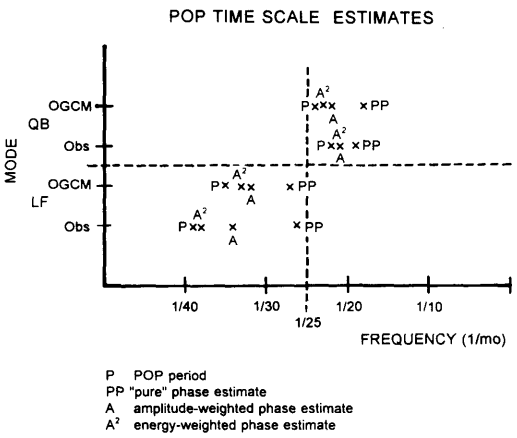

Fig. 9. Time scale estimates for the Low-Frequency and Quasibiennial modes by four different methods from the POPs analysis of the observations (OBS) and OGCM forced by the observed winds OGCM. Note the time scale separation of the two modes and the rather good correspondence between like estimates for the observations and simulation. The symbols are defined on the Figure.

scale estimation is due to the fact that the processes we are studying are broadband in frequency space (but apparently highly peaked in wave number space). Without a dominant spectral frequency peak, it seems unlikely that a characteristic time scale can be defined with high precision.

In a sense, the results presented here on the temporal variability of the PSM are consistent with the hypothesis of Jin et al. (1994) and Tziperman et al. (1994) that ENSO events are essentially chaotic in nature and so no true periodicity is expected. Rather the oscillation might take on different temporal characteristics depending on the background mean state, strength of ocean/atmosphere coupling, etc.

7. Conclusions

A variety of numerical simulations have been carried out in order to investigate the origins of the Principal Spatial Mode (PSM) described in the observational study of Latif et al. (1992), hereafter L92. Considerable effort is expended to show numerically that simulations bear a statistically significant relationship to the observations. The principal results of this study are as follows:

(i) An ocean general circulation model (OGCM) was forced with the observed wind stress over a 29-year period. The fields of SST, sea level and wind stress produced patterns of variability similar to those found in the data (L92). It is clear that the OGCM produces reasonably well the PSM.

(ii) The OGCM was forced by noise that was (a) white in space and time and (b) red in space but white in time. The PSM described in L92 and (i) above was not found in run (a) but was found in the noise simulations (b), whether or not the seasonal cycle of wind stress or the annual average stress were included. This mode is not dependent directly on seasonal cycle forcing, but does require large scale coherent structures in the wind forcing.

(iii) A hybrid coupled model (HCM) consisting of the OGCM noted above and a statistical atmospheric component produced the simulated PSM variations much like those observed in nature and in the run where the OGCM was forced by observed winds. Comparison of this simulation with those described in (ii) show that air-sea interactions both amplify the PSM by a factor of 5–6 over the strength it would have in a totally random (in time) atmosphere, thereby making it climatologically important and supplying the coupling mechanism for the existence of PSM.

(iv) The temporal variability in the simulated PSM depends critically on the seasonality in the strength of the anomalous, near-resonsant coupling between the ocean and atmosphere. This is distinctly different from the assertion that the PSM is driven directly by the annual cycle.

(v) The characteristic time scale one assigns to the simulated PSM can vary from 26–39 months depending on the analysis procedure one uses. Some of these estimates fall into a range of time scales often associated with the tropospheric quasibiennial oscillation. Given the broadband nature of the frequency spectrum in the range from 1 cycle/20 months to 1 cycle/40 months, it seems unlikely that the time scale of the PSM can be more precisely determined.

8. Acknowledgments

Support for this work was provided by the office of Climate Dynamics Program, National Science Foundation under grant NSF ATM93-14495, and

the Scripps Institution of Oceanography. Part of the work was supported by the Bundesminister fur Forschung und Technologie. Thanks are due Tony Tubbs for carrying out most of the calculations required for this paper and to C. Keller of IGPP Los Alamos National Laboratory who made computer time available as part of the University of California's INCOR program.

9. Appendix A

Principal oscillation patterns

Our statistical investigation of the data is based on the method of Principal Oscillation Patterns (POPs) (Hasselmann, 1988; Von Storch et al., 1988; Xu and Von Storch, 1990), which is designed to extract the dominant modes of variability from a multi-dimensional data set. The POPs are the eigenvectors of the system matrix obtained by assuring the data can be represented by a multivariate first order Markov process. POPs are in general complex with real part p_1 and imaginary part p_2. The corresponding complex coefficient time series satisfies the standard damped harmonic oscillator equation, so that the evolution of the system in the two dimensional POP space can be interpreted as a cyclic sequence of spatial patterns ($\cdots \rightarrow p_1 \rightarrow -p_2 \rightarrow -p_1 \rightarrow p_2 \rightarrow p_1 \rightarrow \cdots$). The characteristic period to complete a full cycle will be referred to as "rotation period" and the e-folding time for exponential decay as "damping time". Since the two time scales are estimated as part of the POP analysis, narrow band pass filters to identify the different variability modes in the data are not required. We therefore need less a priori information than in other recent studies (Rasmusson et al., 1990; Barnett, 1991; Ropelewski et al., 1992). Further, since we consider simultaneously both atmospheric and oceanic quantities, the POPs can be regarded as the normal modes of the coupled ocean-atmosphere system under the assumption that the coupled system is well represented as a first order Markov process.

10. Appendix B

Estimating POP time scales

A standard POP analysis can be used in four different ways to estimate the time scales of a data set. The most immediate and standard estimate is obtained directly from the complex eigenvalues of the system matrix (Von Storch et al., 1988; Xu and Von Storch, 1990). These eigenvalues and original data can be used to estimate a POP amplitude ($A(t)$) and incremental phase ($\Delta\phi(t)$), which $\Delta\phi$ is defined to lie between $-\pi$ and π. The incremental phase is the change in POPs phase between successive time increments (Δt). With these definitions, the remaining three ways to estimate time scales for POPs are:

cumulative phase:

$$\left[\frac{1}{2\pi T}\int_0^T |\Delta\phi(t)|\,\mathrm{d}t\right]^{-1};$$

amplitude weighted:

$$\left[\frac{1}{2\pi T}\frac{\int_0^T A(t)\,|\Delta\phi(t)|\,\mathrm{d}t}{\int_0^T A(t)\,\mathrm{d}t}\right]^{-1};$$

energy weighted:

$$\left[\frac{1}{2\pi T}\frac{\int_0^T A^2(t)\,|\Delta\phi(t)|\,\mathrm{d}t}{\int_0^T A^2(t)\,\mathrm{d}t}\right]^{-1}.$$

REFERENCES

Barnett, T. P. 1991. The interaction of multiple time scales in the tropical climate system. *J. Clim.* **4**, 269–285.

Barnett, T. P., Graham, N., Latif, M., Pazan, S. and White, W. 1993. ENSO- and ENSO-related predictability. Part I: Prediction of equatorial Pacific sea surface temperature with a hybrid coupled ocean-atmosphere model. *J. Clim.* **6**, 1545–1566.

Barnett, T. P., Latif, M., Kirk, E. and Roeckner, E. 1991. On ENSO Physics. *J. of Clim.* **4**, 487–515.

Battisti, D. S. 1988. Dynamics and thermodynamics of a warming event in a coupled tropical atmosphere–ocean model. *J. Atmos. Sci.* **45**, 2889–2919.

Battisti, D. S. and Hirst, A. C. 1989. Interannual variability in a tropical atmosphere-ocean model: Influence of the basic state, ocean geometry and nonlinearity. *J. Atmos. Sci.* **46**, 1687–1712.

Bjerknes, J. 1969. Atmospheric teleconnections from the equatorial Pacific. *Mon. Weather Rev.* **97**, 163–172.

Brier, G. W. 1978. The quasi-biennial oscillation and

feedback processes in the atmosphere-ocean-earth system. *Mon. Wea. Rev.* **106**, 938–946.

Cane, M. A., Münnich, M. and Zebiak, S. E. 1990. A study of self-excited oscillations of the tropical ocean-atmosphere. Part I: Linear analysis. *J. Atmos. Sci.* **47**, 1562–1577.

Cane, M. A. and Sarachik, E. S. 1981. The response of a linear baroclinic equatorial ocean to period forcing. *J. Mar. Res.* **39**, 651–693.

Chao, Y. and Philander, S. G. H. 1993. On the structure of the Southern Oscillation and evaluation of coupled ocean-atmosphere models. *J. Climate* **6**, 450–469.

Climate Diagnostics Bulletin, Nos. 90/1–94/12. Available from US Dept. of Commerce, National Oceanic and Atmospheric Administration, National Weather Service/National Meteorological Center, World Weather Building, Room 605, 5200 Auth Rd., Washington, DC 20233.

Goldenberg, S. B. and O'Brien, J. J. 1981. Time and space variability of the tropical Pacific wind stress. *Mon. Wea. Rev.* **109**, 1190–1207.

Graham, N. E., Barnett, T. P., Cane, M. A. and Zebiak, S. E. 1994. Simulated greenhouse warming and model ENSO cycles. *SIO Reference Series no. 94–04.* Available from SIO Library, Scripps Institution of Oceanography, La Jolla, CA 92093.

Graham, N. E. and White, W. B. 1988. The El Niño/Southern Oscillation as a natural oscillator of the tropical Pacific Ocean-Atmosphere system. *Science* **240**, 1293–1302.

Graham, N. E. and White, W. B. 1990. The role of the western boundary in the ENSO cycle: Experiments with coupled models. *J. Phys. Oceanog.* **20**, 1935–1948.

Hasselmann, K. 1988. PIPs and POPs. The reduction of complex dynamical systems using principal interaction and oscillation patterns. *J. Geoph. Res.* **93**, 11015–11021.

Hirst, A. C. 1986. Unstable and damped equatorial modes in simple coupled ocean atmosphere models. *J. Atmos. Sci.* **43**, 606–630.

Horel, J. D. 1982. On the annual cycle of the tropical Pacific atmosphere and ocean. *Mon. Wea. Rev.* **110**, 1863–1878.

Jin, F. F., Neelin, J. D. and Ghil, M. 1994. El Niño on the Devil's staircase: annual subharmonic steps to chaos. *Science* **264**, 70–72.

Latif, M. 1987. Tropical ocean circulation experiments. *J. Phys. Oceanogr.* **17**, 246–263.

Latif, M., Barnett, T. P., Graham, N. and Flügel, M. 1992. *Modal structure of variations in the tropical Pacific climate system, Part I. Observations.* Max Planck Inst. für Meteorologie Rep. No. 91, Hamburg, Germany.

Latif, M., Sterl, A., Maier-Reimer, E. and Junge, M. M. 1993. Structure and predictability of the El Niño/Southern Oscillation phenomenon in a coupled ocean-atmosphere general circulation model. *J. Clim.* **6**, 700–708.

Legler, D. M. and O'Brien, J. J. 1984. *Atlas of tropical Pacific wind stress climatology 1971–1980.* Florida State University, Dept. of Meteorology, Tallahassee, FL.

Meehl, G. A. 1987. The annual cycle and its relationship to interannual variability in the tropical Pacific and Indian Ocean regions. *Mon. Wea. Rev.* **115**, 27–50.

Meehl, G. A. 1992. A coupled air-sea biennial mechanism in the tropical Indian and Pacific regions: Role of the ocean. *J. Clim.* **6**, 31–41.

Miller, A. J., Barnett, T. P. and Graham, N. E. 1993. A comparison of some tropical ocean models: Hindcast skill and El Niño evolution. *J. Phys. Oceanogr.* **23**, 1567–1591.

Neelin, J. D. 1991. The slow sea surface temperature mode and the fast-wave limit: Analytic theory for tropical interannual oscillations and experiments in a hybrid coupled model. *J. Atmos. Sci.* **48**, 584–606.

Neelin, J. D. and Jin, F.-F. 1993. Modes of interannual tropical ocean-atmosphere interaction—a unified view. Part II. Analytical results in the weak-coupling limit. *J. Atmos. Sci.* **50**, 3504–3522.

Neelin, J. D., Latif, M., Alaart, M. A. F., Cane, M. A., Cubasch, U., Gates, W. L., Gent, P. R., Ghil, M., Gordon, C., Lau, N. C., Mechoso, C. R., Meehl, G. A., Oberhuber, J. M., Philander, S. G. H., Schopf, P. S., Sperber, K. R., Sterl, A., Tokioka, T., Tribbia, J. and Zebiak, S. E. 1992. Tropical air-sea interaction in general circulation models. *Climate Dynamics* **7**, 73–104.

Nicholls, N. 1978. Air-sea interaction and the quasi-biennial oscillation. *Mon. Wea. Rev.* **106**, 1505–1508.

Nicholls, N. 1984. The Southern Oscillation and Indonesian sea surface temperature. *Mon. Wea. Rev.* **112**, 424–432.

Pacanowski, R. C. and Philander, S. G. H. 1981. Parameterization of vertical mixing in numerical models of tropical oceans. *J. Phys. Oceanogr.* **11**, 1443–1451.

Philander, S. G. H. 1990. A review of simulations of the Southern Oscillation. *International TOGA Scientific Conference Proceedings*, Honolulu, Hawaii, 16–20 July, 1990. World Climate Research Programme, WCRP-43, WMO/TD-No. 379.

Philander, S. G. H., Pacanowski, R. C., Lau, N. C. and Nath, M. J. 1992. A simulation of the Southern Oscillation with a global atmospheric GCM coupled to a high-resolution, tropical Pacific Ocean GCM. *J. Clim.* **5**, 308–329.

Phillips, O. M. 1962. On the generation of waves by turbulent wind. *J. Fluid Mech.* **2**, 417–445.

Quiroz, R. S. 1983. Relationships among the stratospheric and tropospheric zonal flows and the Southern Oscillation. *Mon. Wea. Rev.* **111**, 143–154.

Rasmusson, E. and Carpenter, T. 1982. Variations in tropical sea surface temperature and surface winds associated with the Southern Oscillation/El Niño. *Mon. Wea. Rev.* **110**, 354–384.

Rasmusson, E. M., Wang, X. and Ropelewski, C. F. 1990. The biennial component of ENSO variability. *J. Mar. Sys.* **1**, 71–90.

Ropelewski, C. F., Halpert, M. S. and Wan, X. 1992. Observed tropospheric biennial variability and its relationship to the Southern Oscillation. *J. Clim.* **5**, 594–614.

Schopf, P. S. and Suarez, M. J. 1988. Vacillations in a coupled atmosphere-ocean model. *J. Atmos. Sci.* **45**, 549–566.

Trenberth, K. E. 1975. A quasi-biennial standing wave in the Southern Hemisphere and interrelations with sea surface temperature. *Quart. J. Roy. Meteor. Soc.* **101**, 55–74.

Tziperman, E., Stone, L., Cane, M. A. and Jarosh, J. 1994. El Niño chaos: Overlapping of resonance between the seasonal cycle and the Pacific ocean-atmosphere oscillator. *Science* **264**, 72–74.

Von Storch, H. 1988. *Climate simulations with the ECMWF T-21 Model in Hamburg*, p. 265. (available from Meteorological Institute, University of Hamburg, Hamburg, Germany).

Xu, J.-S. and Von Storch, H. 1990. Principal oscillation patterns, the state of the ENSO cycle. *J. Climate* **3**, 1316–1329.

Yasunari, T. 1989. A possible link of the QBO's between the stratosphere, troposphere, and sea surface temperature in the tropics. *J. Meteorol. Soc. Japan* **67**, 483–493.

Zebiak, S. and Cane, M. 1991. Greenhouse gas induced climate change: a critical appraisal of simulations and observations, M. E. Schlesinger (ed.). Elsevier Press, NY.